HELICAL MICRO-HOLE DRILLING OF CHEMICALLY STRENGTHENED GLASS USING CAPSULE-SHAPED ELECTROPLATED DIAMOND TOOL

M.S.A. Aziz[1], A. Mizobuchi[2], R. Izamshah[1], M.S. Kasim[1], E. Mohamad[1], M.R. Salleh[1] and T. Ishida[2]

[1]Faculty of Manufacturing Engineering, Universiti Teknikal Malaysia Melaka, Hang Tuah Jaya, 76100 Durian Tunggal, Melaka, Malaysia.

[2]Graduate School of Technology, Industrial and Social Sciences, Tokushima University, 2-1 Minami-Josanjima, Tokushima 770-8506, Japan.

Corresponding Author's Email: [2]a-mizobuchi@tokushima-u.ac.jp

ABSTRACT: This study investigates the micro-hole drilling performance of chemically strengthened glass plate by using a capsule-shaped electroplated diamond tool and the helical drilling method. Three different helical pitch conditions were tested to drill holes with a diameter of 1 mm. The number of drilled holes, grinding force, and maximum crack size were measured along with the observation of the drilled holes to evaluate the performance of the micro-hole drilling. From the experimental results, it was found that as the size of helical pitch decreased, the number of drilled holes increases where the average grinding force generated becomes smaller. By using small helical pitch condition, 43 holes could be drilled but the maximum crack size generated at the outlet side of the drilled hole is not able to achieve the high-grade quality compared to the inlet side. The resultant grinding force generated when the tool tip nearing the outlet side of the glass plate has caused the large crack at a certain position on the outlet side.

KEYWORDS: *Micro-Hole Drilling; Helical Drilling Method; Chemically Strengthened Glass; Electroplated Diamond Tool; Maximum Crack Size*

1.0   INTRODUCTION

Chemically strengthened glass (CSG) is a type of glass where the surface is strengthened with a micro-layer of residual compressive stress through a chemical strengthening treatment [1]. The layer of residual compressive stress acts to suppress crack propagation from scratches formed on the glass surface. Therefore, CSG is durable and has strength approximately five times higher than the glass made from

thermal tempering method [2]. In recent years, the demand for CSG has been used as a protective film for LCD panels, such as smartphones and tablets. The protective film for these electronic devices requires through-hole drilling techniques for certain parts, such as phone speakers, proximity sensors, and cameras to function well. However, in order to make a through-hole in a CSG film or plate, a cutting edge, which is stronger than the compressive stress of the glass surface, is necessary. In addition, the smaller residual tensile stress within the CSG makes it brittle and easily propagates cracks. Therefore, it is very difficult to process a through-hole in a CSG plate.

A through-hole drilling method which applies an axial ultrasonic vibration to a milling tool using an ultrasonic device has shown great potential in drilling CSG, where it reduces the thrust force, tool wear and average chipping size [3-7]. Moreover, micro-hole drilling using electro discharge machining, electrochemical discharge machining and air abrasive air also can produce precise holes on glass [8-12]. However, these methods have a higher cost and complicated setup. It is a favourable if there is a simpler processing method by using conventional machining tools that can perform the through-hole drilling process of CSG. Previously, several types of electroplated diamond tools have been developed and successfully used for the through-hole drilling of soda-lime glass with high precision [13-14]. However, performing the through-hole drilling of CSG using the electroplated diamond tool with higher precision was still difficult and needs further improvements [15]. Thus, in this study, a helical drilling method is applied to the capsule-shaped electroplated diamond tool to perform the through-hole drilling of CSG. This study investigates the hole drilling performance with varied helical pitch.

2.0   METHODOLOGY

2.1   Chemically Strengthened Glass (CSG) Used as a Workpiece

The CSG plate (Corning Inc.) with the geometry of 50×50×1 mm was used as the workpiece in this study. Figure 1 illustrates the stress distribution within the CSG plate from the cross-section view. As indicated in the figure, the inner part of the glass plate that comprises the tensile stress (TS = 40 MPa) is sandwiched between layers of high compressive stress, CS = 759 MPa and depth of layer, DOL = 48 μm, which is the result of strengthening by ion exchange. The mechanical properties of CSG plate are described in Table 1 with inclusion of soda lime glass (SLG) mechanical properties as a reference. The CSG and

SLG plates have almost similar values in terms of the density, Young's Modulus, Poisson's ratio, shear modulus and Vickers hardness before the ion strengthening process. However, after undergoing this process, the CSG plate is about five times stronger than the SLG plate.
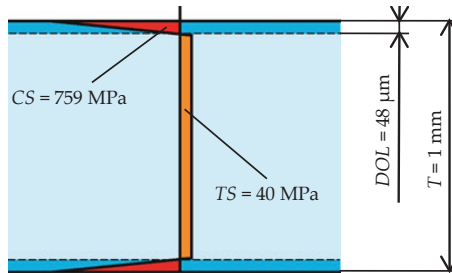

Figure 1: Stress distribution within CSG plate from cross-section view

Table 1: Mechanical properties of CSG and SLG

| PARAMETERS	CSG	SLG
Density [g/cm³]	2.39	2.5
Young's modulus [GPa]	69.3	73
Poisson's ratio	0.22	0.21
Shear modulus [GPa]	28.5	30
Vickers hardness (200g load) [kgf/mm²]		
Non-strengthened	534	533
Strengthened	649	580
Fracture toughness [MPam$^{0.5}$]	0.66	-
Critical load [N]	150	10
Load to failure (ring on ring) [N]	1225	216
Coefficient of expansion (0-300°C) [/°C]	75.8×10^{-7}	85×10^{-7}

2.2 Capsule Shaped Electroplated Diamond Tool

Figure 2 shows the 2D drawing and the SEM image of the capsule-shaped electroplated diamond tool used in this research. The tool is constructed by a 3 mm diameter of the shaft, a hemispherical shaped tool tip with a diameter of 0.74 mm, and a part connecting the shaft and the tool tip with a diameter of 0.5 mm. The tool shaft is made from cemented carbide (WC: 90 wt%, Co: 10 wt%) as the tool tip is coated with an average size of 28 μm of diamond abrasive grains (#600) through the nickel electroplating process.
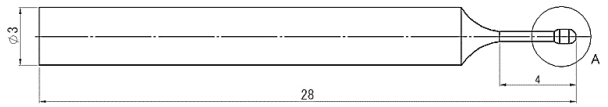
(a) Overall view
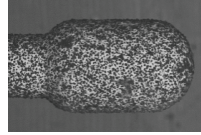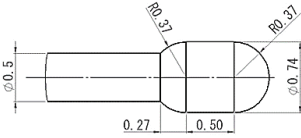
(b) Close-up view of part A (tool tip)   (c) SEM image of the tool tip

Figure 2: 2D drawing and SEM image of electroplated diamond tool

2.3   Helical Drilling

Figure 3 shows a schematic diagram of helical drilling using a capsule-shaped tool. The helical drilling combines two rotational movements simultaneously; the rotational motion of the tool itself (tool rotation) and the revolution motion of the spindle (spiral motion). It is completed by moving the tool towards the z-axis direction in a spiral movement, which synchronises with circular interpolation of the x-y plane. The distance from the centre axis of the machined hole to the tool centre axis is referred to as the radius of the helical trajectory (r_h). Since the diameter of the capsule-shaped tool is 0.74 mm, r_h is set to 0.13 mm to form a hole with a diameter of 1 mm. Helical pitch (h_p) is the feed rate towards the z-axis direction when the tool completes one circular motion with the feed rate of the helical trajectory (f_a) and the feed rate of the tool axis direction (f). The open space created between the tool and the inner surface of the drilled hole acts as the chip discharge area during the helical drilling process.
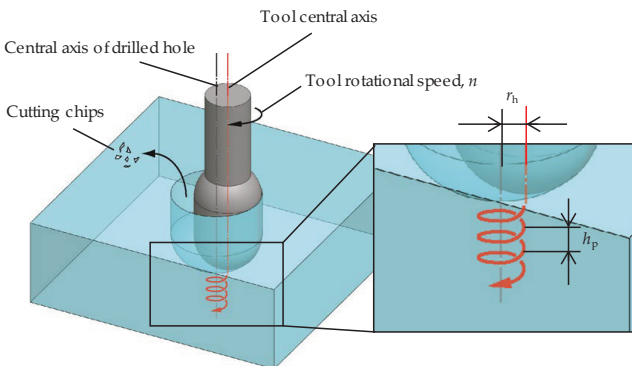

Figure 3: Schematic diagram of helical drilling

2.4   Experimental Setup

The experimental setup for the helical micro-hole drilling is shown in Figure 4. The CSG plate used as the workpiece is fixed by a special jig with grooves. The grinding force during the helical drilling process is measured by using a three-component force dynamometer which is fixed under the jig. The helical drilling process is performed by using a CNC milling machine, but since its spindle rotation speed can only achieve up to 4000 rpm, a high-speed air spindle is attached to the original spindle. The high-speed air spindle is controlled by a control unit and can be set from 5000 to 50000 rpm. The capsule-shaped tool is installed onto the high-speed spindle and fed towards the grooves of the jig to allow the tool to penetrate the glass plate. A water-soluble coolant, which is diluted about ten times with tap water is used and supplied directly to the processing point.
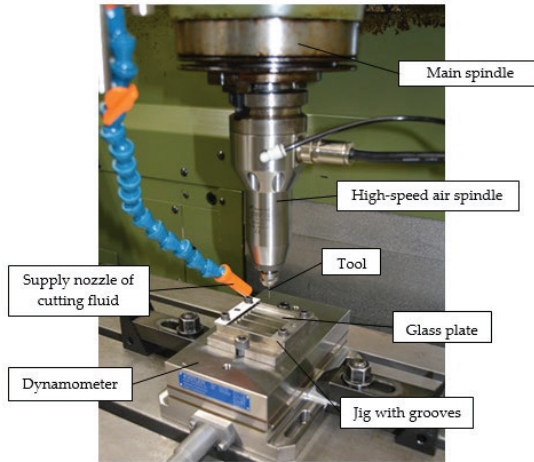

Figure 4: Experimental setup

Table 2 summarises the machining conditions used in this study. The high-speed spindle rotational speed (n) and the feed rate of f are constant at 20000 rpm (cutting speed 46.5 m/min) and 1 mm/min, respectively. In order to drill a 1 mm diameter of the hole, the radius of the r_h is set to 0.13 mm. h_p is varied into 0.1 mm, 0.05 mm and 0.01 mm, which gives the values of the feed rate of the f_a as 8.1 mm/min, 16.3 mm/min and 81.7 mm/min, respectively by using the following equation:

$$f = \frac{h_p}{2\pi r_h} \times f_a \tag{1}$$

Table 2: Machining conditions

Spindle rotational speed n [rpm]	20000		
Radius of the helical trajectory r_h [mm]	0.13		
Helical pitch h_P [mm]	0.1	0.05	0.01
Feed rate of the helical trajectory f_a [mm/min]	8.1	16.3	81.7
Feed rate of the tool axis direction f [mm/min]	1		

3.0   RESULTS AND DISCUSSION

3.1   Effects of Different Helical Pitch on Machining Performance

Table 3 shows the appearance of the first drilled hole at the inlet and outlet sides of the glass plate by drilling with varied helical pitch values. As shown in the table, the hole drilling with the highest helical pitch (0.1 mm) led to a broken glass as a crack occurred during the hole drilling process. Holes are successfully drilled using the helical pitch of 0.05 mm and 0.01 mm but the glass broke on the third and 43rd drilled hole, respectively. It was found that under each condition, there is no adhesion of chips onto the tool tip and the cylindrical part after the hole drilling process finished, which indicates that the chip discharge performance using the helical drilling method is excellent.

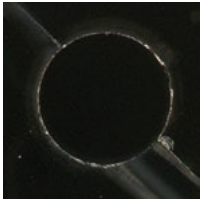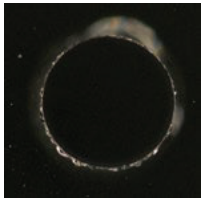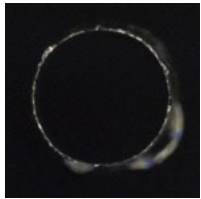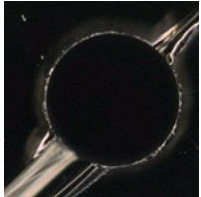Table 3: Appearance of the drilled hole by using varied helical pitch
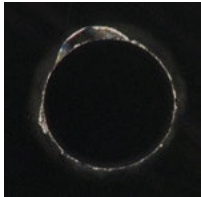
Helical pitch, h_P [mm]	0.1	0.05	0.01
Inlet			
Outlet			

Figure 5 shows the profiles of the three-component grinding forces (F_x, F_y, and F_z) recorded when drilling the first hole for each helical pitch condition. Similarities were found in all three conditions where the grinding force (F_z) rises as soon as the machining started (machining depth = 0) due to the increase of the contact area between the tool and

the glass plate as the hemispherically shaped tool tip starts to penetrate. From the machining depth of 0.2 mm, the F_z changes almost constantly and before reaching the depth of 1.0 mm, it decreases sharply to almost zero. Otherwise, the profiles of F_x and F_y repeat a constant cycle but with a phase difference of $\pi/2$. Those cycles coincide with the revolution cycle of the helical motion and gradually decrease until zero from the moment of the decrease of F_z.
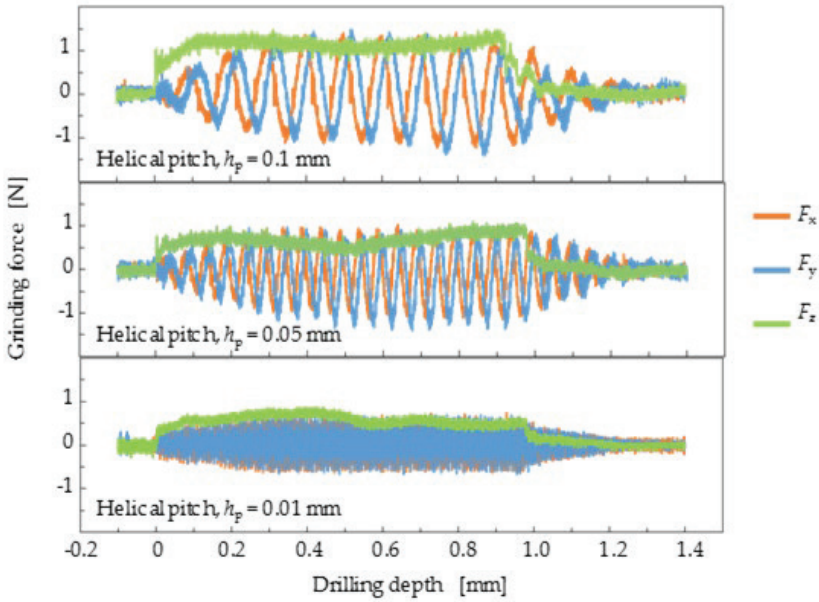

Figure 5: Profiles of the three-component grinding force
(first drilled hole)

The resultant force (R) is derived from the three-component grinding force measured by the piezoelectric dynamometer, and R can be obtained from the following equation and the vectors of each force are explained in Figure 6.

$$R = \sqrt{F_x^{\,2} + F_y^{\,2} + F_z^{\,2}} \qquad (2)$$

Figure 7 shows the relationship between the number of drilled holes and R for each drilled hole. The magnitude of R is calculated from the average value of the resultant force recorded from the machining depth of 0.4 to 0.9 mm. The resultant forces for the first hole drilled using the helical pitch of 0.1, 0.05 and 0.01 mm are 1.60 N, 1.14 N, and 0.72 N, respectively. Drilling with a smaller helical pitch resulted in a smaller resultant force, as it required a lower force to machine a smaller

feed amount in the tool axis direction for each tool revolution. It also can be understood from this result that there is a tendency to achieve a higher number of drilled holes with smaller grinding force but the force gradually increases as the number of drilled hole increases due to the tool wear.
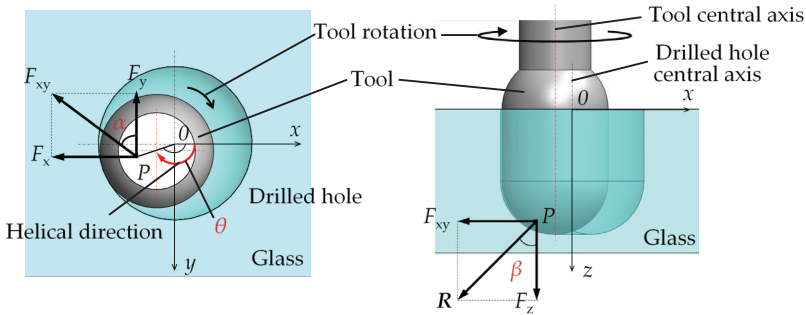

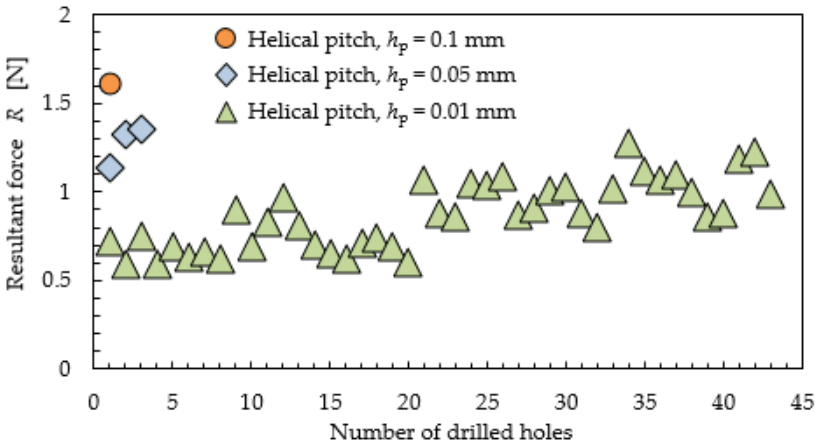Figure 6: Vectors of the component forces and the resultant force at *P* point

Figure 7: Resultant force when drilling with varied helical pitch condition

3.2 Micro-Hole Drilling Performance using Small Helical Pitch

As indicated in the previous result, the capsule-shaped electroplated tool can drill up to 43 holes when drilling with small helical pitch (h_p = 0.01 mm). Figure 8 shows the maximum crack size at the inlet and outlet sides of a glass plate with the increment number of drilled holes using the small helical pitch condition and the appearances of the inlet and outlet sides of the 5th, 10th, 20th and 30th drilled holes are indicated in Table 4. From Figure 8, the average of the maximum crack size at the

inlet and outlet sides are 0.033 mm and 0.176 mm, respectively. The chipping size generated at the outlet side is five times larger than that of the inlet side.
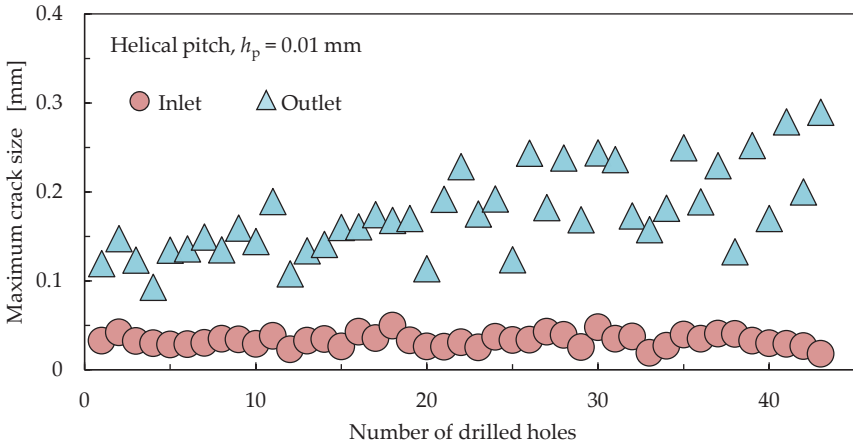

Figure 8: Maximum crack size at the inlet and outlet sides of drilled holes

Table 4: Appearance of the drilled hole with the increment number of holes

Number of drilled hole	5th	10th	20th	30th
Inlet				
Outlet				

From the observation of the appearance of the drilled holes (shown in Table 4), cracks generated at the inlet side are almost constant even with the increment number of drilled holes. However, cracks generated at the outlet side were found to be revolved at a certain position and the size increases as the number of drilled holes increases. In this study, the micro-hole drilling process is considered as a high grade if

the maximum crack size is less than 0.1 mm for drilling a hole with a diameter of 1 mm. The maximum crack size generated at the inlet side worked well with the high-grade machining quality, which is less than 0.1 mm. However, the maximum crack size generated at the outlet side of the drilled hole has exceeded 0.1 mm, which is far from achieving the high-grade machining quality.

3.3   Crack Progression at the Outlet Side of Plate

As mentioned above, the large crack generated at the outlet side of the glass plate was found only at a certain position. To understand the mechanism of such crack, grinding force profile at the position when the tool tip penetrated the outlet side of the glass plate was enlarged as shown Figure 9. From the figure, it was found that F_z starts to decrease drastically at Q point but both F_x and F_y are constantly changing. The appearance of glass plate from the outlet side view before and after the drastic change of F_z is shown in Figures 10(a) and 10(b), respectively. The F_z starts to decrease since the hole of glass plate has been penetrated where the contact area between the tool tip and glass plate becomes smaller. However, at the same time, the large crack was propagated by the resultant force, which diverged from the z-axis direction. The large crack still remains after the hole drilling is completed as indicated in Figure 10(c).
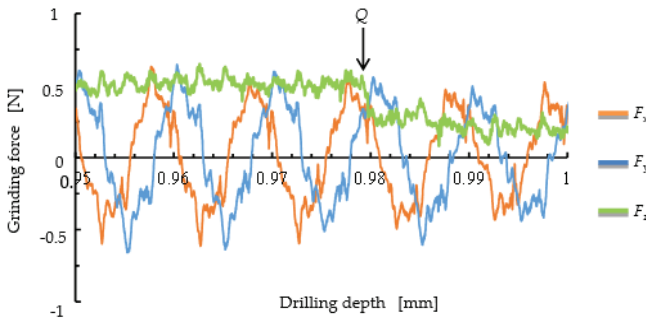

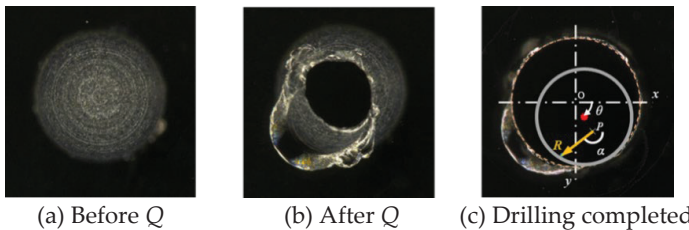Figure 9: Grinding force profiles at the position nearing the outlet side

(a) Before Q (b) After Q (c) Drilling completed

Figure 10: Appearance of drilled hole during tool penetration from the outlet side view

Figure 11 shows the relationship between the F_z and the depth penetration of Q point with the increment number of drilled holes. From the figure, it is understood that as the number of drilled holes increases, F_z also increases which is caused by the influence of tool wear. However, the depth penetration of Q point decreases which means that the depth of the tool penetration becomes shallow as the number of drilled holes increases. As previously shown in Figure 6, vector R is diverging from the x-axis direction with an angle of β. If the depth of tool penetration is shallow, the resultant force will generate larger crack which corresponds with the results indicated in Table 4.
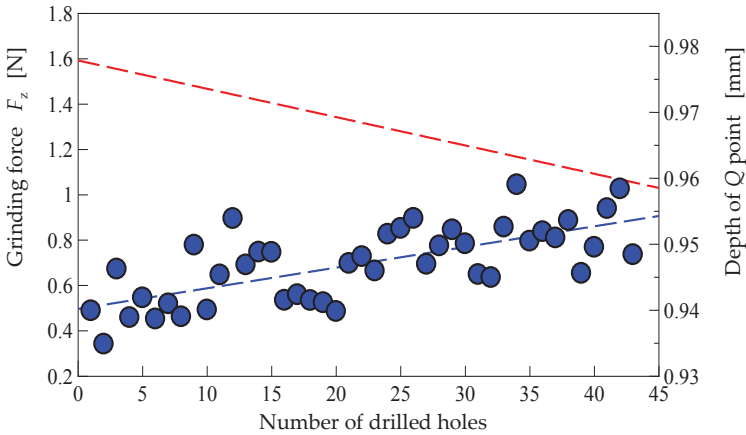

Figure 11: Relationship between F_z and Q point

4.0   CONCLUSION

In this paper, a capsule-shaped electroplated tool was used to perform micro-hole drilling on chemically strengthened glass plate using the helical drilling method. Varied helical pitch conditions were tested to investigate the micro-hole drilling performance. The results obtained in this study are summarised below.

i.   Drilling with smaller helical pitch resulted in smaller resultant force and a higher number of drilled holes since it required a lower force to machine smaller feed amount in the tool axis direction for each tool revolution.

ii.   The maximum crack size generated at the inlet side worked well with the high-grade machining quality, which is less than 0.1 mm, but the maximum crack size generated at the outlet side of the drilled hole exceeded 0.1 mm, which is far from achieving the high-grade machining quality.

iii.   As the number of drilled holes increases, grinding force F_z also increases, but the depth of the tool penetration becomes shallow which was the factor that the large cracks revolved at a certain position of the outlet side of CSG.

ACKNOWLEDGMENTS

REFERENCES

[1]   R.E. Smallman and R.J. Bishop, *Modern Physical Metallurgy and Materials Engineering*. Oxford: Butterworth-Heinemann, 1999.

[2]   D. Uhlmann and N.J. Kreidl, *Elasticity and Strength in Glasses: Glass: Science and Technology*. USA: Academic Press, 2012.

[3]   K. Noma, Y. Kakinuma, T. Aoyama and S. Hamada, "Ultrasonic vibration-assisted machining of chemically strengthened glass with workpiece bending", *Journal of Advanced Mechanical Design, Systems, and Manufacturing*, vol. 9, no. 2, pp. JAMDSM0016-JAMDSM0016, 2015.

[4]   K. Noma, Y. Takeda, T. Aoyama, Y. Kakinuma and S. Hamada, "High-precision and high-efficiency micromachining of chemically strengthened glass using ultrasonic vibration", *Procedia CIRP*, vol. 14, pp. 389-394, 2014.

[5]   K. Noma, Y. Kakinuma, T. Aoyama and S. Hamada, "A Study on Slotted Hole Processing of Chemically Strengthened Glass Using Ultrasonic Vibration", in Proceedings of JSPE Semestrial Meeting, Tottori, Japan, 2014, pp. 629-630 (in Japanese).

[6]   K. Egashira, R. Kumagai, R. Okina, K. Yamaguchi and M. Ota, "Drilling of microholes down to 10 μm in diameter using ultrasonic grinding", *Precision Engineering*, vol. 38, no. 3, pp. 605-610, 2014.

[7]   J. Wang, P. Feng, J. Zheng and J. Zhang, "Improving hole exit quality in rotary ultrasonic machining of ceramic matrix composites using a compound step-taper drill", *Ceramics International*, vol. 42, no. 12, pp. 13387-13394, 2016.

[8]   S.T. Chen, Z.H. Jiang, Y.Y. Wu and H.Y. Yang, "Development of a grinding–drilling technique for holing optical grade glass", *International Journal of Machine Tools and Manufacture*, vol. 51, no.2, pp.95-103, 2011.

[9] Y. Xu, J. Chen, B. Jiang and J. Ni, "Investigation of micro-drilling using electrochemical discharge machining with counter resistant feeding", *Journal of Materials Processing Technology*, vol. 257, pp.141-147, 2018.

[10] C.T. Yang, S.S. Ho and B.H. Yan, "Micro hole machining of borosilicate glass through electrochemical discharge machining (ECDM)", *Key Engineering Materials*, vol. 196, pp.149-166, 2001.

[11] J.B. Madhavi and S.S. Hiremath, "Investigation on Machining of Holes and Channels on Borosilicate and Sodalime Glass using μ-ECDM Setup", *Procedia Technology*, vol. 25, pp.1257-1264, 2016.

[12] H. Li, J. Wang, N. Kwok, T. Nguyen and G.H. Yeoh, "A study of the micro-hole geometry evolution on glass by abrasive air-jet micromachining", *Journal of Manufacturing Processes*, vol. 31, pp.156-161, 2018.

[13] K. Honda, A. Mizobuchi and T. Ishida, "Investigation of Grinding Fluid for Prevention of Chip Adhesion in Miniature Drilling of Glass Plate Using Electroplated Diamond Tool", *Key Engineering Materials*, vol. 749, pp. 52-57, 2017.

[14] A. Mizobuchi, K. Honda and T. Ishida, "Improved Chip Discharge in Drilling of Glass Plate Using Back Tapered Electroplated Diamond Tool", *International Journal of Precision Engineering and Manufacturing*, vol. 18, no. 9, pp. 1197-1204, 2017.

[15] A. Mizobuchi, Y. Kagawa and T. Ishida, "Miniature Drilling of Chemically Strengthened Glass Plate Using Electroplated Diamond Tool", *International Journal of Automation Technology*, vol. 10, no. 5, pp. 780-785, 2016.